International Journal of Environmental Sciences
ISSN: 2229-7359
Vol. 11 No. 6, 2025
https://theaspd.com/index.php

Dual Functionality Of Cobalt Doped Nickel Oxide Nanoparticles In Treatment Of Waste Water Free From P-Nitrophenol And Microbes

Venkata Nagendra Kishore T[1], K. Jaya Prasanthi[1]*, B.N. Suresh Varma Dendukuri[3], P Seetharam[2], Jayasree Komara[1]
[1]Department of Chemistry, AU College of Science & Technology, Andhra University, Visakhapatnam, Andhra Pradesh-530003, India.
[2]Bio Enviro Chemical Solutions, Visakhapatnam, Andhra Pradesh-530003, India.
[3]Department of Chemistry, Sri Vishnu Engineering College for Women, Bhimavaram, Andhra Pradesh-534201, India.
*Corresponding author email: dr.kjprasanthi@andhrauniversity.edu.in

Abstract
Wastewater treatment is critical for mitigating the environmental impacts of industrial and domestic effluents while conventional treatment technologies effectively reduce organic load and nutrient concentrations in nanotechnology. This study critically examines the dual impacts of wastewater treatment technologies emphasizing the potential of Co–NiO NPs to advance sustainable low-carbon and high-performance effluent remediation. The desirable NPs were prepared hydrothermally and their properties were investigated using XRD, SEM, EDS, BET, UV-Vis, TGA, XPS and FTIR techniques. The average particle size of NiO NPs and Co-NiO NPs are 14.58nm and 7.06nm respectively. The UV absorbance studies shown a strong absorption at 370nm and 375nm respectively and the band gap energy values of NiO NPs and Cu-NiO NPs are 3.36eV and 3.30eV. The doping of cobalt in to the NiO NPs had decreased the band gap energy(3.36eV) resulting that Co-NiO NPs can show more effectiveness in removal of PNP. In addition to that the Co-NiO NPs bioactivity was tested against three bacterial strains E.coli, B.coagulans and A.niger shown to be more effective. Optimization of the adsorption process was conducted by modulating the agitation length of 120 minutes with the Co-NiO NPs dose of 0.1 gm, the solution pH of 5 and the PNP starting concentration of 10 mg/L resulted in a 100% conversion of PNP degradation rate and on the other hand A.niger shown enhanced antifungal activity with zone of inhibition(ZOI) 16mm compared to NiO NPs ZOI with 13mm.

Keywords: *Co-NiO NPs, Hydrothermal, Antimicrobial activity, para-nitro phenol, Photocatalytic dye degradation.*

1. INTRODUCTION

Water is an indispensable resource for all forms of life yet its quality is increasingly compromised by industrialization, urbanization and anthropogenic activities. Among the various contaminants discharged into aquatic systems organic pollutants and pathogenic microorganisms pose serious risks to both ecological and human health. One such hazardous pollutant is *para*-nitrophenol (PNP) a highly toxic compound extensively used in the manufacturing of pesticides, pharmaceuticals, dyes and explosives [1]. Due to its high water solubility, persistence and bio accumulative potential PNP has been classified as a priority pollutant by the U.S. Environmental Protection Agency [2]. Exposure to PNP can result in severe health effects such as hemolytic anemia, liver dysfunction and neurological damage [3].

Simultaneously, the presence of pathogenic microorganisms in water sources including *E.coli, S.aureus and P.aeruginosa* contributes to widespread outbreaks of waterborne diseases [4]. The increasing antibiotic resistance among these bacteria has rendered traditional treatment processes less effective [5]. While conventional wastewater treatment methods such as activated sludge processes, chlorination and ozonation offer partial solutions they often fall short in completely removing recalcitrant pollutants like PNP and inactivating resistant microbial populations [6].

In this context, the emergence of nanotechnology has provided new opportunities for advanced water treatment solutions. Nickel oxide (NiO) nanoparticles in particular have gained attention due to their unique physicochemical properties such as wide bandgap (~3.6–4.0 eV), chemical stability, high surface energy and redox activity which make them suitable for both photocatalytic degradation and antimicrobial applications [7,8]. NiO nanoparticles can degrade organic pollutants under UV or visible light via photocatalysis and adsorb them onto their surface through electrostatic and π-π interactions [9]. Furthermore, NiO nanoparticles are known to produce reactive oxygen species (ROS) such as hydroxyl radicals and superoxide ions which cause oxidative stress in microbial cells leading to membrane damage and cell death [10].

However, pristine NiO nanoparticles may suffer from drawbacks such as particle agglomeration, limited visible-light response and low charge separation efficiency [11]. To overcome these limitations metal ion doping has emerged as an effective strategy to tailor the electronic structure, surface area and catalytic activity of NiO nanoparticles. Transition metals such as cobalt (Co), copper (Cu) and zinc (Zn) have been successfully used to dope NiO enhancing its photocatalytic efficiency, antibacterial potential and pollutant adsorption capacity [12-14]. For instance, Co-doped NiO NPs exhibit improved oxygen vacancy concentration and visible light absorption, while Cu-doped variants show enhanced antimicrobial activity due to increased ROS production [15].

Various synthesis methods such as sol–gel, hydrothermal, co-precipitation and green synthesis using plant extracts have been employed to fabricate doped NiO nanoparticles with controlled morphology and size which further influence their environmental applications [16,17].

This study aims to synthesize and characterize both pure and cobalt-doped NiO NPs evaluating their dual capability in the removal of *para*-nitrophenol and the inactivation of pathogenic microorganisms in wastewater. Key operational parameters such as adsorbent dose, pH, contact time and initial pollutant concentration will be optimized to achieve maximum remediation efficiency. In parallel, the antibacterial activity will be assessed by analyzing the zone of inhibition (ZOI) surrounding bacterial colonies in the presence of nanoparticles. The proposed work intends to elucidate the mechanism of action of doped nanoparticles and establish their potential as multifunctional nanomaterials for advanced water purification systems.

2.Experimental section

2.1.Materials used

The following chemicals are AR grade with 98% procured from Merck company, India includes Nickel chloride hexahydrate ($NiCl_2{\cdot}6H_2O$), Sodium hydroxide (NaOH), Cobalt chloride ($CoCl_2$), Ethanol(C_2H_5OH) and Ascorbic acid($C_6H_8O_6$). Doubled distilled water was used throughout the studies.

2.2. Synthesis of Co-doped NiO NPs

1.78 gm of $NiCl_2$ (0.25M)was dissolved in 30 mL of deionized water and kept it for 10 min stirring. Then, 30 mL of 0.12gm of NaOH solution (0.1 M) was gradually added to the above solution. Then the mixture was kept on the hotplate allowed to stirring and heated at 60°C for 30 min. To the above mixture, 0.4gm of $CoCl_2$ (0.1M) 30 mL was added and kept for 30 min stirring followed by adding a pinch of ascorbic acid and kept it for one hour stirring. Then it is transferred into a Teflon stainless steel beaker and placed in a muffle furnace at 180°C for 4 hours. After this, it was allowed to cool until it reaches the room temperature and filtered, washed the obtained mixture with water and ethanol and finally dried it in oven at 60°C for 8 hours and the product was grinded to fine powder for further analysis. In the absence of $CoCl_2$, the same procedure was repeated in synthesizing the Nickel oxide nanoparticles (NiO NPs)

2.3. Antibacterial activity

2.3(a). Test Microorganisms

The antibacterial efficacy of the synthesized materials was assessed using standard bacterial strains: *B.coagulans*(MTCC-5856), *E.coli*(MTCC-589) and *A.niger*(ATCC-16404). These strains were procured from the Microbial Type Culture Collection (MTCC), Institute of Microbial Technology (IMTECH), Chandigarh, India. Upon receipt, the bacterial cultures were sub cultured on freshly prepared nutrient agar slants and maintained at 4 °C for short-term use. For long-term preservation cultures were stored at −20 °C in nutrient broth supplemented with 15% (v/v) glycerol.

2.3(b). Preparation of Muller-Hinton Agar Medium

Muller Hinton Agar Medium (High-Media) was dissolved in water in 500 mL conical flask and was sterilized in an autoclave at 121°C, 15lbs for 15 min and poured in sterilized petri plates. The antibacterial activity of sample was evaluated by Agar Well diffusion Method (Perez et al., 1990). Inoculum were spread over the surface of agar plates with sterile cotton swab. Nutrient broth was prepared by dissolving 13 g of dehydrated nutrient medium in 1 L of distilled water with continuous heating to ensure complete dissolution. The prepared medium was aliquoted into appropriate containers and sterilized by autoclaving at 121°C and 15 psi for 15 minutes. The broth was used for bacterial culture propagation during antibacterial assays.

2.4.Anti-microbial activity

Muller Hinton Agar Medium (High-Media) was dissolved in water in 500 mL conical flask and was sterilized in an autoclave at 121°C, 15 lbs. for 15 min and poured in sterilized petri plates. The antibacterial activity of sample was evaluated by Agar Well diffusion Method (Perez et al., 1990). Inoculum were spread over the surface of agar plates with sterile cotton swab. To test the antibacterial activity of Sample, aliquots of compounds (100µl/mL, 50µl/mL, 10µl/mL of 1mg/mL concentration) were directly pipetted into the wells which were already been inoculated with specific species i.e., Gram-ve *(E.coli)*, Gram+ve *(B.coagulans)*, Fungal *(A.niger)* and then plates were incubated for a period of 24 h at 37°C in an incubator and the diameter(mm)of the clear inhibitory zone formed around the discs was measured.

2.5. Characterization

In this present study the characterization were carried out using the following techniques X-ray diffraction (XRD) study was carried out with instrument D8 Bruker Advance A25, Cu tube using its wavelength with Cu-Kα =1.5418 A° in the range 2θ from 10° - 80° to determine the interplanar spacing of the nanoparticles , Fourier transformation Infrared spectroscopy (FTIR) analysis with the instrument ATR-FTIR spectrophotometer with make Bruker, model Alpha-II, Air-cooled, 12V, 20W beam Splitter Zinc Selenide (ZnSe) in the range 4000-500cm^{-1}, Quantachrome NOVA touch 4 LX instrument was used for BET analysis using nitrogen isotherms at 77 K, Tecnai T20, 200Kev, FEI electron microscope was used for the TEM analysis, The XPS (X ray photoelectron spectroscopy) analysis was carried out with the instrument Omicron ESCA make Oxford Germany. TGA was carried out using Hitachi STA 7300 model from 30°C to 1000°C temperature, the lateral size and morphology of the nanomaterials were described by using scanning electron microscope (FE-SEM, Quanta 450 FEG, FEI, USA; and SEM, Hitachi SU1510, Japan) at an operating voltage of 10–30 kV.

2.6.Measurement of photocatalytic activity

The photocatalytic experiments were conducted under ambient atmospheric conditions at different pH value 3,5,7, 9 and 11 solutions using Philips mercury lamp UV (A) 365 nm, contains four lamps off 15 W for each one as the light source. For each run 30, 50 and 100mg of catalyst powders was dispersed in 100 mL of aqueous solution of *para*-Nitro phenol(PNP) with a concentration of (10 mg L^{-1}). Prior to the beginning of irradiation, the mixture was allowed to equilibrate in the dark with stirring for 30 min. At certain irradiation intervals, aliquots of about 3 mL solution were withdrawn from the suspension and then centrifuged. The photocatalytic performance of the sample was subsequently gauged by measuring intensity changes of the optical absorbance peaks at 375nm, of aqueous supernatant aliquots containing PNP using a UV-visible spectrophotometer.

The conversion efficiency (%)of the photodegradation process was calculated with the relation

$$\text{Conversion efficiency(\%)} = \left(\frac{A_{PNP}^{0}-A_{PNP}}{A_{PNP}^{0}}\right) X\ 100 \qquad \text{.................. Eqn (1)}$$

Where A_{PNP}^{0} is the initial concentration of PNP and A_{PNP} is the concentration of PNP at a certain irradiation time. The variation of PNP concentration as a function of irradiation time, under visible light was determined using the UV-Visible spectroscopy based on a calibration curve.

3. Characterization techniques

3.1. X-Ray Diffraction analysis

The X-ray diffraction (XRD) analysis was used to identify the crystalline structure of the synthesized material. The existence of strong and sharp diffraction peaks of the NiO NPs with 2θ values found to be 19.11°, 31.65°, 33.16°, 38.38°, 45.37°, 51.42°, 59.40°, 62.83° and 69.93° [18] were shown in figure 1. Co-NiO NPs exhibited the (2θ) at 19.06°, 33.11°, 33.16° 38.12°, 45.70°, 51.42, 59.27°and 69.27° which corresponding well to the (101), (110),(200) ,(111), (200) (311), (220) and (400)planes respectively, matched with of cubic NiO indicating a face-centered cubic (FCC) structure. There are no other peaks were observed in between peaks ,confirmed that these are free from the impurities.

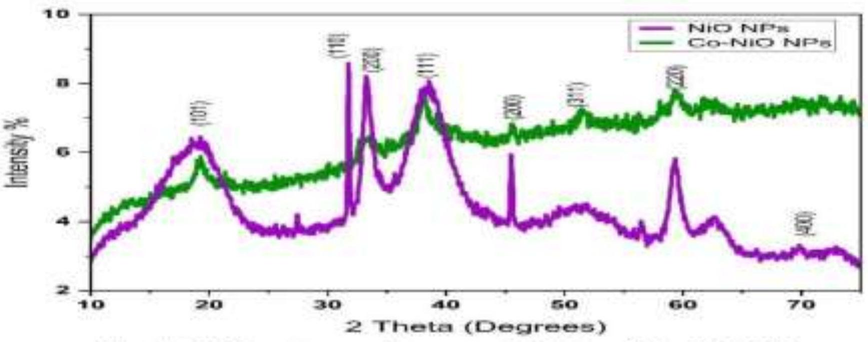

Fig.1: XRD patterns of prepared NiO and Co-NiO NPs

The average crystalline size(D) of hydrothermally prepared materials was measured by Deby-Scherer formula (Eqn 2) obtained as 14.58nm for NiO and for the Co- doped NiO is 7.06nm.

$$D = \frac{k\lambda}{\beta Cos\theta} \qquad \text{.................. Eqn (2)}$$

where 'λ' means the X-radiation wavelength, 'k' represents the Scherrer's constant (0.94), 'β' is the full width at half maximum (FWHM) and 'θ' denotes the diffraction angle.

3.2.Fourier transform Infra- Red spectral analysis:

Figure 2 aims the FTIR spectra of NiO nanoparticles, which showed the several significant absorption peaks at 3637,3380,1625,1348,1035,613 and 503 cm^{-1} and after doping the Cobalt into NiO slight decrease in the vibrational frequency is observed resulting that the composition was not changed even doping. The broad absorption band in the region of 650–500 cm^{-1} is assigned to Ni-O stretching vibration mode; the broadness of the absorption band indicates that the NiO powders are nanocrystals[19]. The vibrations could be seen from that the broad absorption at 3380 cm^{-1} is attributes to the band O-H stretching vibrations and the weak band near 1625 cm^{-1} is assigned to H-O-H bending vibrations were also presented due to the adsorption of water in air.

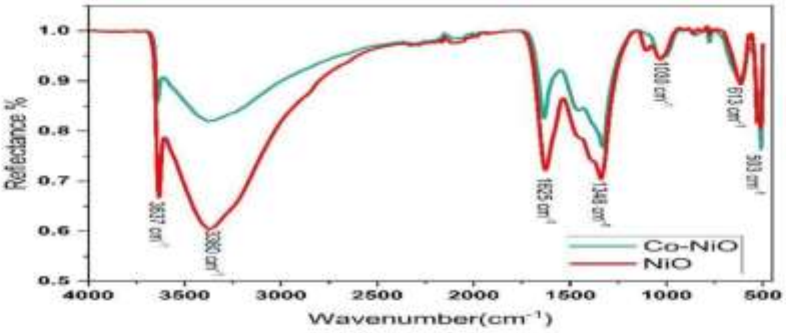

Fig.2: FTIR patterns of prepared NiO and Co-NiO NPs

These observations provided the evidence to the effect of hydration in the structure. Meanwhile, it implied the presence of hydroxyl in the precursor and the broad absorption around 1030 cm^{-1} is assigned to the band C-O bond stretching vibrations.

3.3. Scanning electron microscopy

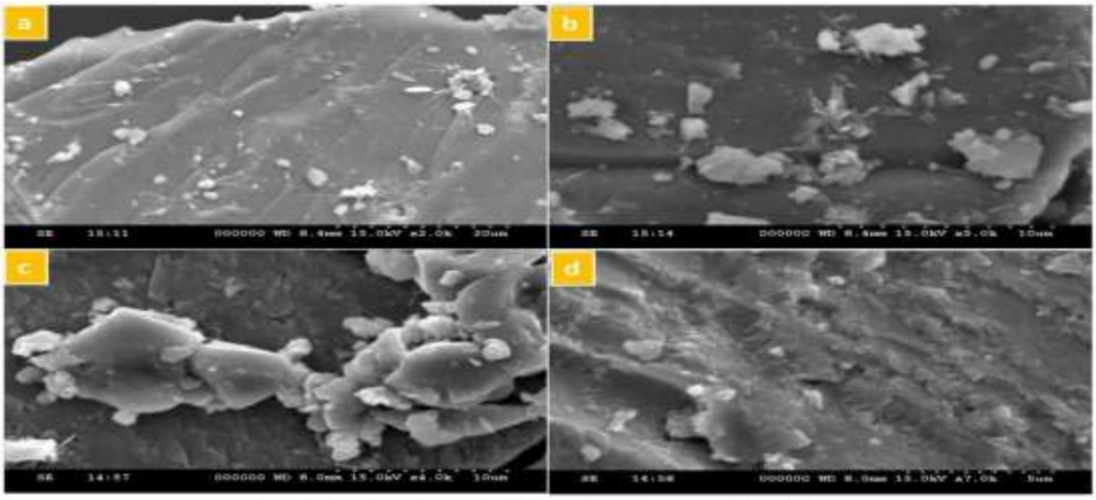

Fig.3: SEM images (a, b) NiO (c, d) Co-NiO NPs

The surface morphology of the synthesized pure NiO and Co-doped NiO nanoparticles was investigated using scanning electron microscopy (SEM). The SEM images in figure(3) revealed that the nanoparticles were well-dispersed exhibiting a cubical shape with high crystallinity [20]. Both the pure NiO NPs and Co-NiO NPs samples displayed comparable morphological characteristics. However, some degree of agglomeration was observed likely due to the aggregation or overlapping of smaller particles forming nanoparticle clusters. This observation is in close agreement with previous studies which reported an average particle size distribution of approximately 18nm. Notably, the pure NiO nanoparticles appeared smaller in size, whereas Co doping resulted in a relatively larger particle size. This finding correlates well with XRD analysis which confirmed an increase in particle size upon Cobalt incorporation in to NiO.

3.4. Energy Dispersive X-Ray Spectroscopy analysis (EDS

The hydrothermally synthesized Co-NiO NPs were subjected to elemental analysis using Energy Dispersive X-ray Spectroscopy (EDS) integrated into a Quanta 450 FEG, USA system. Additionally, spectral signals corresponding to Nickel(Ni), Oxygen(O)

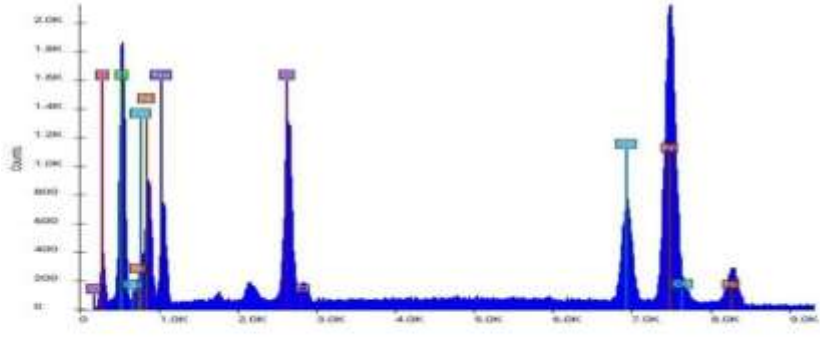

Fig.4: EDS analysis of Co-NiO NPs

and Cobalt(Co) were detected. The elemental composition of pure Nickel and Oxygen was obtained as 47.90 and 26.60 by weight percentage in NiO NPs and after doping with cobalt the obtained Co-NiO NPs contains Co, Ni and O as 2.75, 29.14 and 34.45 by weight percentage respectively[21]

3.5. Transmission electron microscope

The size and morphology of the nanoparticles were further characterized by TEM. Transmission electron microscope images of the Co-NiO NPs are shown in Fig. 5(a-e). The TEM image of the NiO NPs is obtained with a diameter of 38.1nm after doping the Co-NiO NPs shows uniform particles with a diameter of about 36.2 nm. The SAED pattern given in the Fig.5f show that the obtained Co-NiO NPs are crystalline in nature. Noticed that the mean particle size determined by TEM values of Co-NiO NPs was concurred with XRD crystalline size.

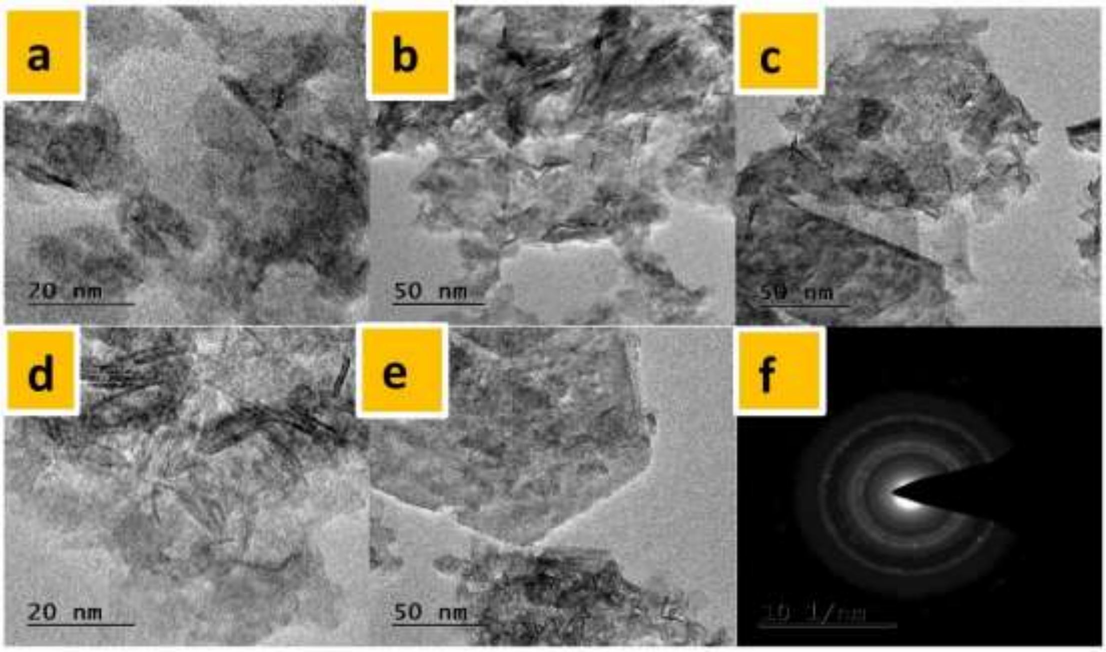

Fig.5: (a-e) TEM images and (f) SAED pattern of Cu-NiO NPs

3.6. BET Surface Area and Porosity Analysis

The N_2 gas adsorption-desorption isotherms obtained from Brunauer–Emmett–Teller (BET) gas sorption analysis reveal that the specific surface area of pure NiO nanoparticles is approximately 109.36 m^2/g while that of cobalt-doped NiO nanoparticles (Co–NiO NPs) increases to 114.86 m^2/g. The pore volume distribution is found to be 0.0241177 cc/g for NiO and 0.0273392 cc/g for Co–NiO indicating enhanced mesoporosity upon doping. Both samples exhibit a Type-IV isotherm with an H3-type hysteresis loop, which is characteristic of mesoporous materials [22,23]. The average pore diameter is calculated to be 3.05887 nm for NiO NPs and 3.4179 nm for Co–NiO NPs suggesting that cobalt doping slightly increases pore size possibly due to lattice distortions and altered crystal growth kinetics during synthesis. The increase

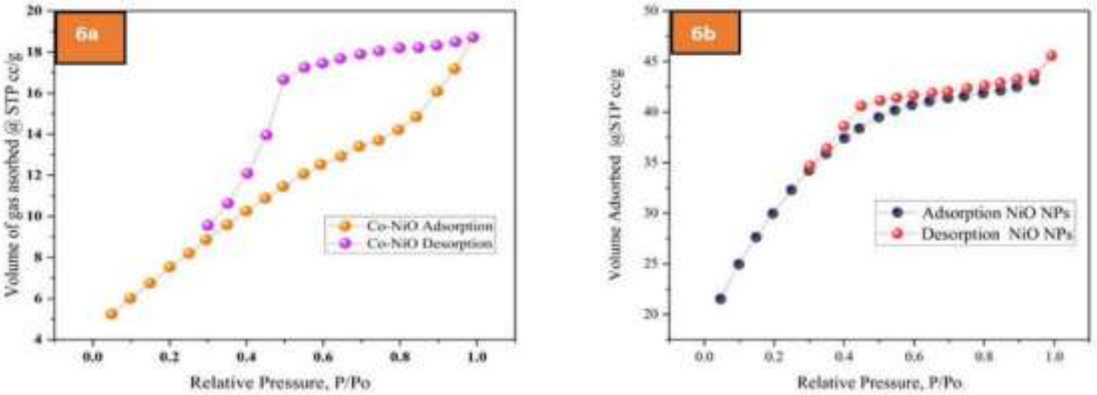

Fig: 6a & 6b represents the adsorption/desorption of Co-NiO & NiO NPs in adsorbed N_2 volume at STP (cc/g) observed in Co–NiO samples supports the conclusion of an enhanced surface area. The approximately 5% increase in surface area upon Co doping directly correlates with improved active surface sites which is critical for applications in catalysis, photocatalysis and adsorption-based wastewater treatment [24–26].The BET surface area and porosity analysis clearly indicate that cobalt doping enhances the structural properties of NiO nanoparticles. The increase in surface area and pore volume improves the accessibility of reactive sites which is beneficial for catalytic and adsorption applications. The mesoporous nature and Type-IV isotherm further support the high potential of Co–NiO NPs in surface-dependent processes such as photocatalytic degradation and antibacterial activity in wastewater treatment systems.

3.7. X-ray Photoelectron Spectroscopy (XPS) Analysis

X-ray Photoelectron Spectroscopy (XPS) was employed to investigate the elemental composition and electronic states of both undoped NiO and cobalt-doped NiO (Co–NiO) nanoparticles. For pristine NiO NPs the core-level binding energy for O1s was recorded at 530.0 eV and for Ni $2p_{3/2}$ at 855.0 eV which are characteristic of Ni^{2+} species in NiO and lattice oxygen [27].Upon cobalt doping the XPS spectra of Co–NiO NPs showed additional peaks at 780.0 eV and 795.0 eV corresponding to the Co $2p_{3/2}$ and Co $2p_{1/2}$ orbitals respectively. These values confirm the presence of Co^{2+} ions consistent with prior studies [28]. The Ni $2p_{3/2}$ and Ni $2p_{1/2}$ peaks remained at 855.0 eV and 872.0 eV respectively while the O 1s peak slightly shifted to 529.5 eV possibly due to the altered chemical environment caused by the incorporation of cobalt into the NiO lattice [29].All observed peaks closely match reported literature values validating the oxidation states and confirming the successful doping of Co^{2+} ions without any significant formation of secondary phases. Furthermore, the elemental distribution confirmed through EDS analysis correlates well with the XPS results indicating the absence of extraneous or contaminant elements. The detailed XPS spectra are shown in Figure 7(a–d).

3.8. Thermogravimetric analysis

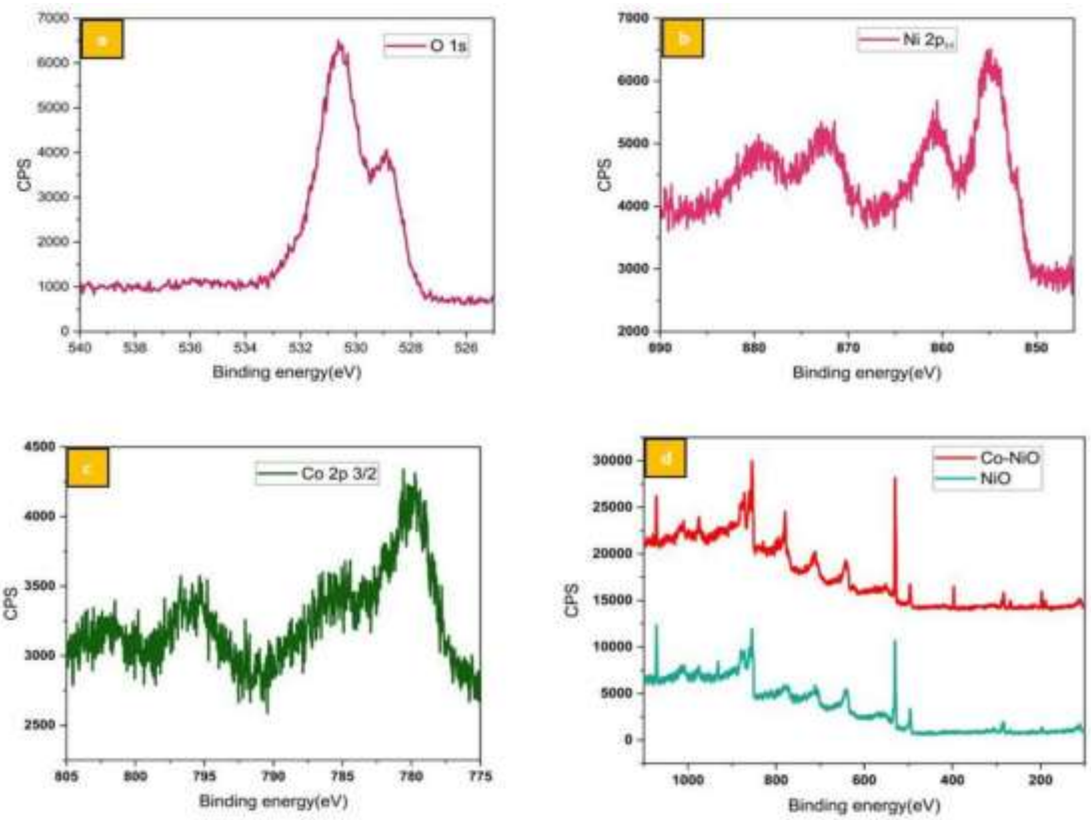

Fig.7: XPS data a) O 1s b) Ni 2p3/2 c) Cu 2p3/2 d) Cu-NiO NPs and NiO NPs

The thermal behavior of Co-NiO NPs was analyzed using thermogravimetric (TG) analysis, as shown in Figure 8. The TG curve exhibits discrete weight losses at different temperature ranges. The first decomposition occurs between 38°C and 116°C with an endothermic peak at 78°C corresponding to the loss of lattice water. A significant weight loss is observed from room temperature to 307°C with a total mass reduction of 15.06% attributed to the conversion of water molecules present in the internal molecular lattice. The strong weight loss was noticed in the decomposition process through multiple stages of hydrothermally prepared Co-NiO NPs at 3.8%(6.014mg), 16.37%(5.029mg) and 16.78%(4.18gm). The thermal decomposition is completed at 892°C, after which the Co-NiO NPs remain as the final product with no further weight loss. For comparison of Co-NiO NPs ,the TG Corves of annealed NiO at 321°C were also analyzed[23]. The results show that Co-NiO NPs exhibit greater thermal stability compared to undoped NiO NPs.

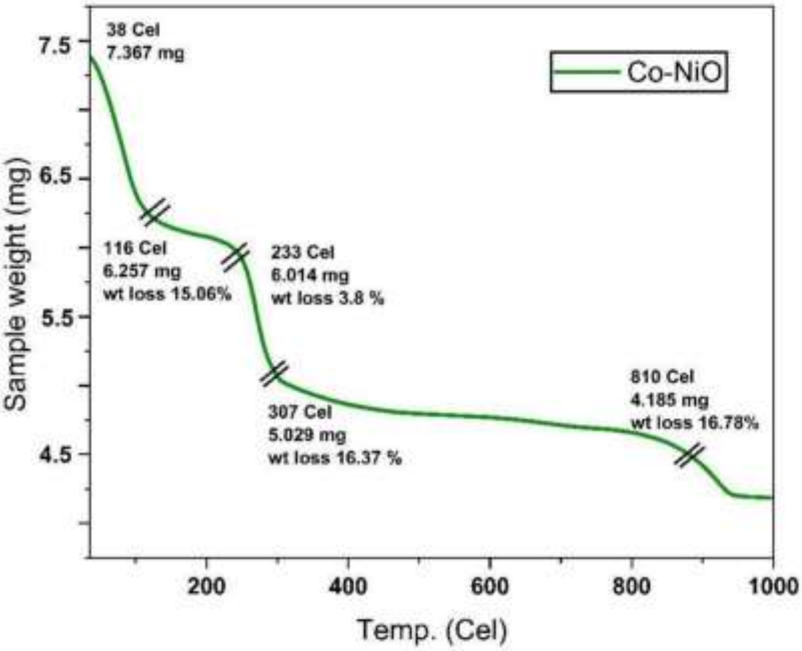

Fig.8: Plots of TGA of Co-NiO NPs ranging from 0°C -1000°C

3.9. UV-Visible spectral analysis

UV-Vis spectral analysis has been done for the prepared samples of bare NiO and Co-NiO NPs and this was shown in Fig.9. NiO NPs show an adsorption edge at 370 nm while Co-NiO NPs show absorption edge above 390 nm due to doping of cobalt. The band gap for nickel oxide to be 3.6 eV[30]. In addition, the band gap energy for pure

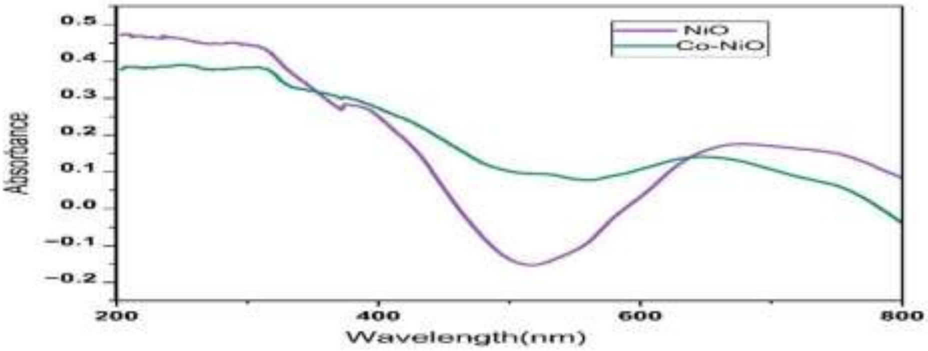

Fig.9: Plots of UV-Visible spectrum of NiO NPs and Co- NiO NPs

NiO NPs was found to be 3.36 eV. Co-NiO NPs which show absorption edge at 375 nm and band gap energy was found to be 3.30eV. The decrease in the band gap energy indicates that maybe it can show more catalytic activity.

4.1.Photocatalytic percentage conversion and conversion of para nitro phenol(PNP)

The photocatalytic performance of hydrothermally prepared NiO and Co-NiO NPs was executed under visible light irradiations is shown in figure 10a & 10b respectively, against PNP at standard conditions like pH-9 catalyst loading and concentration. Initially, the photocatalytic experiment was carried out with bare NiO NPs under similar conditions found to be 38.6% conversion in 120 min. As we expected in enhancement of conversion rate further tested with Co-NiO NPs 100 mg catalyst loading at similar conditions of initial concentration at 5 ppm showed better PNP conversion performance than NiO(38.6%). In order to assess the complete conversion of PNP using prepared Co-NiO NPs, there is necessity to optimize the experiment conditions such as pH, catalyst loading and dye initial concentration.

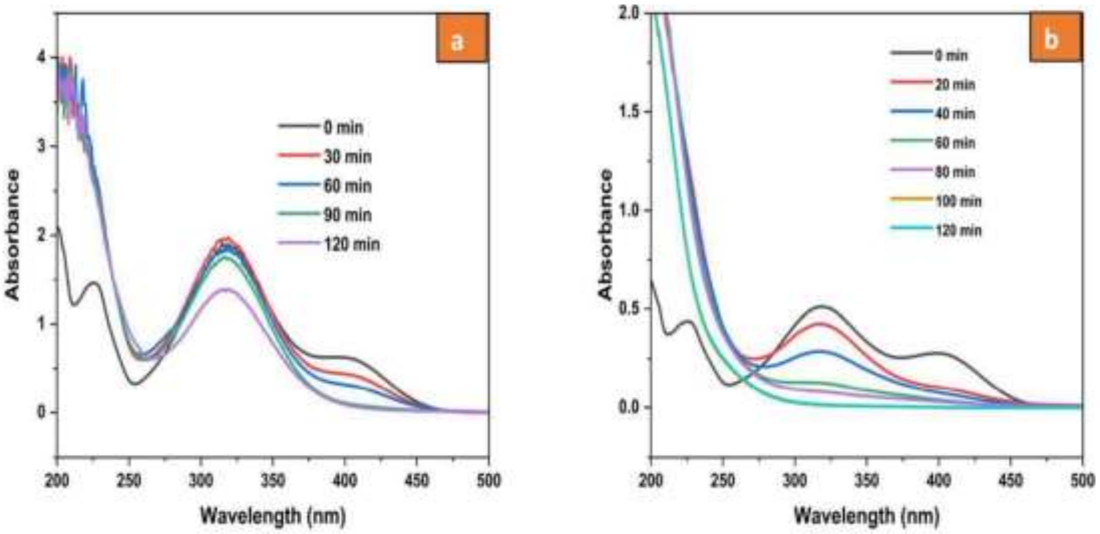

Fig 10 (a, b) PNP conversion using (a) NiO and (b) Co-NiO

a. Effect of pH on PNP conversion

The conversion efficiency of PNP decreases with pH, showing 86% conversion at pH 3, 98.4% at pH 5, 73% at pH 7, 58% at pH 9 and 37% at pH 11 as shown in figure 11. This trend suggests that acidic conditions favour PNP conversion likely due to enhanced hydroxyl radical (•OH) formation and improved oxidation potential. In acidic conditions, high amount of hydroxyl radicals may be available limiting conversion efficiency.

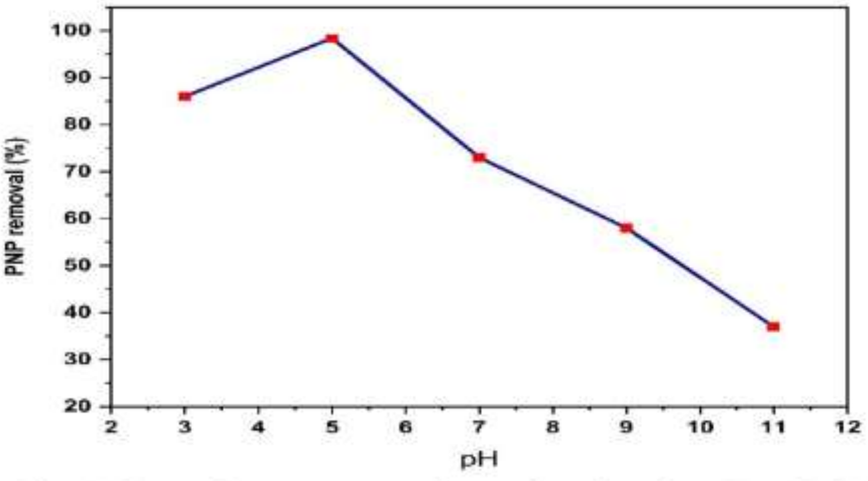

Fig 11:Conversion percentage of para nitro phenol at pH – 3,5, 7, 9

To further optimize the process, decreasing the pH value slightly below 11 could enhance conversion, although excessively less pH levels (< 7) might destabilize the PNP or interfere with catalyst activity

Since pH 5 has shown the highest conversion optimizing reaction time and catalyst dosage is crucial as excessive amounts may lead to radical scavenging and reduced efficiency.

b. Effect of initial PNP concentration

The effect of the organic pollutant concentration on the conversion ability of the Co-NiO NPs as catalyst was studied at an optimized pH-5 and an irradiation time of 120 min by changing the initial PNP concentration of 5, 10, 15, 20 and 30 ppm. The PNP solution containing Co-NiO NPs was kept in the dark for 30 min to achieve the adsorption—desorption thermally between Co-NPs surface and PNP equilibrium. The percent conversion of PNP solution ranging from 5 ppm to 30 ppm was found to be around 25% after the 30 min adsorption and the conversion completed in 120 minutes for 5ppm and 150 minutes in 30ppm. Nearly 30% of the PNP get removed by changing the initial concentration from 5 to 30 ppm. Figure 12 clearly shows that the conversion proficiency of the catalyst is inversely related to the initial concentration of the PNP. As the initial concentration of PNP increases the time needed for complete conversion increases and conversion efficiency decreases. At a high concentration of a PNP maximum number of molecules are adsorbed on the catalyst surface resulting in reduced light penetration[31].

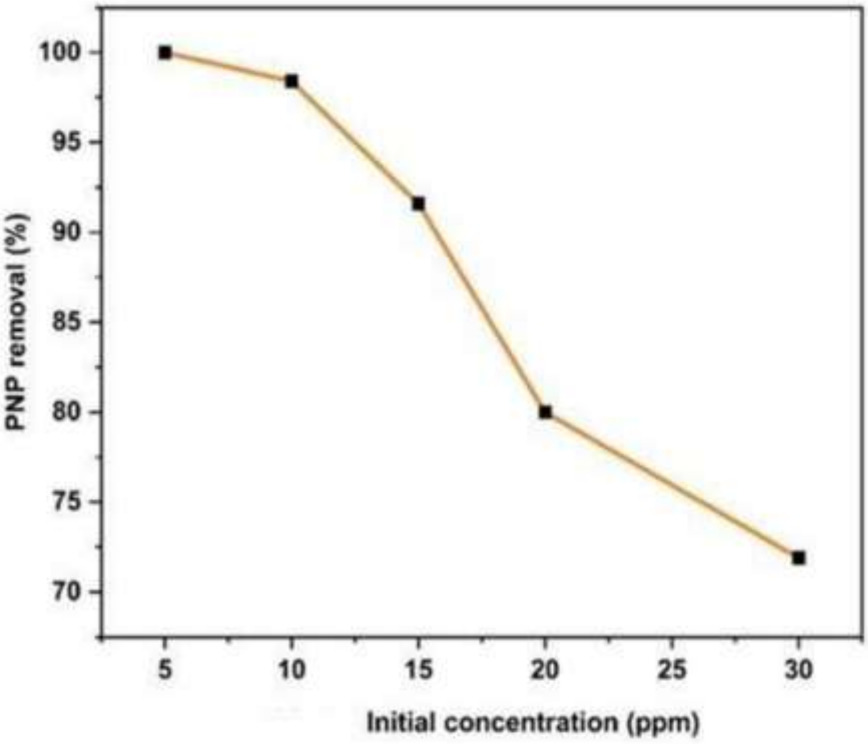

Fig 12: Effect of PNP initial concentration

c. Effect of catalyst dose

The effect of photocatalyst mass on conversion of PNP was studied keeping other experimental conditions constant. The percentage conversion was studied under different Co-NiO NPs catalyst amounts of 30- 70mg with increment of 10mg at constant. Figure 13 exhibits the PNP conversion percentage was increased with catalyst loading amount increases up to 60mg. The number of photons absorbed and the number

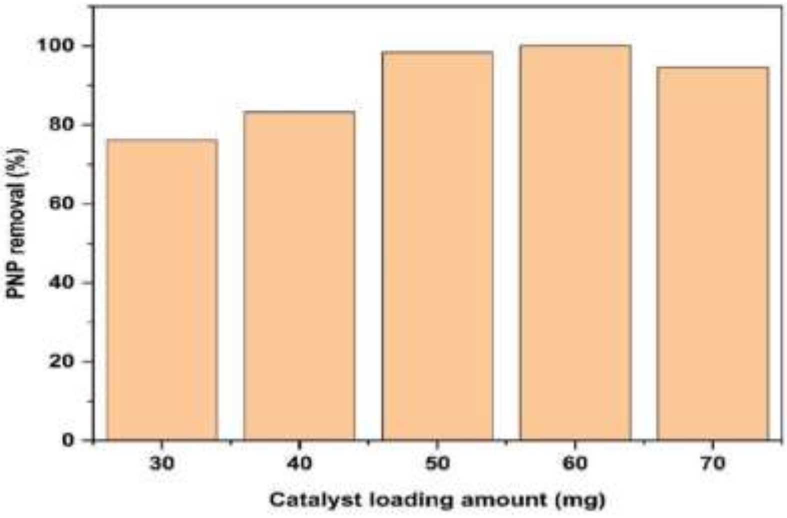

Fig 13: PNP removal with different catalyst dosage

of PNP molecules removed were increased with the increase in catalyst concentration except in 70mg due to agglomeration of Co-NiO NPs. The efficiency goes on increasing with catalytic load due to the uniform dispersion of the catalyst and the availability of more active sites on the surface of the catalyst.

The antimicrobial activity of NiO NPs and Co-NiO NPs were systematically evaluated against representative bacterial and fungal strains using the agar well diffusion method was shown in the table 1. *B.coagulans* exhibiting a slightly higher ZOI (15 mm) than NiO NPs (14 mm) at 100 µl/mL. This enhancement may be attributed to improved surface reactivity and higher positive surface charge due to cobalt incorporation which strengthens electrostatic interactions with the negatively charged bacterial cell membranes leading to better disruption of membrane integrity at higher concentrations. In contrast, the Gram-negative bacterium *E.coli* showed greater susceptibility to pure NiO NPs which produced a maximum inhibition zone of 20 mm at 100 µl/mL whereas Co-NiO NPs showed reduced activity (15 mm). The diminished activity of Co-NiO NPs against *E.coli* may result from the structural differences in Gram-negative bacteria where the outer membrane acts as a barrier to nanoparticles and may limit electrostatic attraction and subsequent penetration. Gram-negative bacteria possess an additional lipopolysaccharide layer that can hinder nanoparticle interaction reducing antibacterial efficiency particularly when surface properties are altered by doping. On the other Co-NiO NPs demonstrated significantly enhanced antifungal activity against *A.niger* with a ZOI of 16 mm compared to 13 mm for NiO NPs at 100 µl/mL. This improved antifungal activity can be linked to increased generation of reactive oxygen species (ROS) enhanced surface area and strong electrostatic interactions between the nanoparticle surface and fungal cell walls.

Table 1. Antibacterial Activity of the NiO NPs and Co-NiO NPs Sample

Test micro-organism	Anti-bacterial activity			
	NiO NPs		Co-NiO NPs	
	Concentration (µl/mL)	Zone of Inhibition (mm)	Concentration (µl/mL)	Zone of Inhibition (mm)
B.coagulans	Control	23	Control	23
	100	14	100	15
	50	13	50	13
	10	12	10	8
E.coli	Control	23	Control	23
	100	20	100	15
	50	15	50	12
	10	12	10	10

A.niger	Control	23	Control	23
	100	13	100	16
	50	10	50	12
	10	8	10	10

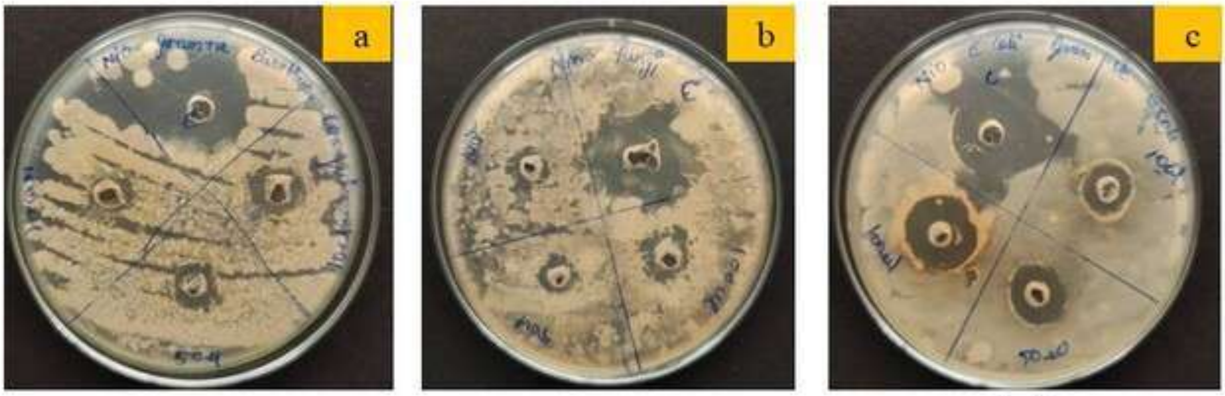

B.coagulans *A. niger* *E.coli*

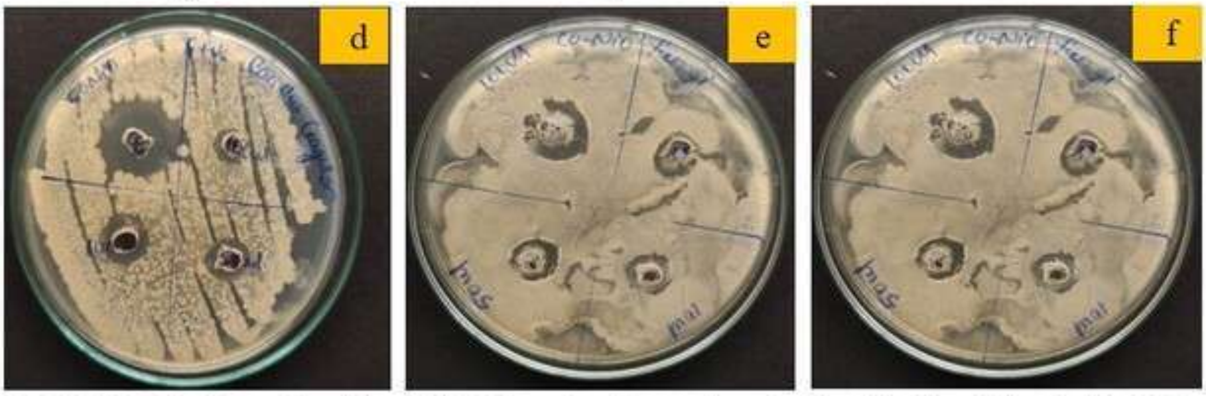

Fig 14: (a,b,c)Anti bacterial activity of NiO NPs against *B.coagulans*, *A.niger*, *E.coli* and (d, e, f) with Cobalt doped NiO NPs against *B.coagulans*, *A.niger*, *E.coli* .

Table-2: Showing the characterization data of the synthesized NiO NPs and Co-NiO NPs

Sample	Crystal size (nm)	Particle size(nm)	Band gap energy (eV)	Surface area (m^2/gm)	Thermal weight Loss (Percentage)
NiO NPs	14.58	38.1	3.6	109.36	22
Co-NiO NPs	7.6	36.2	3.4	114.86	16.37

5. Probable Mechanism of PNP conversion

An important parameter in the photocatalytic reactions taking place on particulate surfaces is the pH of the solution, since it dictates the surface charge properties of the photo catalyst and size of aggregates it forms. Hence, pH plays an important role both in the characteristics of PNP and in the reaction mechanisms that can contribute to conversion namely hydroxyl radical attack, direct oxidation by the positive hole and direct reduction by the electron in the conducting band. In the presence of photocatalyst, it is presumed that the photocatalytic processes are probably result from the electron hole pairs formed on the surface of the semiconductor by the irradiation of the visible light. Then the holes with the high oxidative potential either direct oxidize the reactive dye or react with the OH^- to form hydroxyl radical. When these highly oxidized species like hydroxyl radical($OH^\cdot$) and oxygen radical ($O_2^\cdot$) react with the PNP and produce carbon dioxide and water.

Semiconductor + hν → (semiconductor) $e^-_{CB} + h^+_{VB}$ .... Eqn (3)

h^+_{PNP} + PNP → $PNP^{\cdot +}$ (oxidation of PNP) ....Eqn (4)

$h^+_{PNP} + OH^- \rightarrow OH^\cdot$

$OH^\cdot$ + PNP → degradation of the PNP → CO_2 + H_2O ...Eqn (5)

The degradation of PNP using different metal doped nanoparticles which were synthesized through deposition–precipitation, sol-gel, and hydrothermal methods were shown in table 2. The most effective catalyst was Co–NiO NPs synthesized hydrothermally achieving complete (100%) conversion within 120 minutes. These findings underscore the influence of dopant type, synthesis method and activation conditions on the photocatalytic efficiency of nanoparticles.

Table 3 : Showing the data of differently synthesized metal oxide nanoparticles formation and their percentage of dye degradation.

S. No	System	Metal Doped	Method	Particle Size (nm)	Degradation (%)	Time	Reference
1	5% Co–NiO	Co	Green (plant extract)	~80	–	–	[32]
2	Ni–Co LDH	Co + Ni	Co-precipitation	Varies	~100	Minutes	[33]
3	$Co_{0.4}Ni_{0.6}Fe_2O_4$ ferrite	Co + Ni + Fe	Reverse micelle	4–6	~99	~20 min	[34]
4	5% Co–NiO	Co	Hydrothermal	~25	–	–	[35]
5	Co–NiO (10% Co)	Co	Sol–gel	~15–30	85–95	1–2 hr	[36]
6	Co–NiO nanosheets	Co	Hydrothermal + calcination	~50 × 200	~92	30 min	[37]
7	Electro spun Co–NiO nanofibers	Co	Electrospinning	~100	~90	45 min	[38]
8	Co–NiO quantum dots	Co	Pulsed laser ablation	3–5	–	–	[39]
9	Magnetic Co–NiO core–shell	Co	Co-precipitation + annealing	50	95	1 hr	[40]
10	Co–NiO with graphene oxide	Co + GO	Solvothermal	~20–40	98	25 min	[41]
11	Mesoporous Co–NiO	Co	Soft-templating sol–gel	~10–50	94	30 min	[42]
12	Co–NiO–carbon nanocomposite	Co + C	Hydrothermal + pyrolysis	~15	~97	20 min	[43]
13	Microwave-synthesized Co–NiO	Co	Microwave-assisted	~20–30	90	15 min	[44]
14	Co–NiO via combustion synthesis	Co	Solution combustion	~30–60	88	1 hr	[45]
15	Co–NiO with carbon nanotubes (CNT)	Co + CNT	Hydrothermal	~25	96	22 min	[46]

S. No	System	Metal Doped	Method	Particle Size (nm)	Degradation (%)	Time	Reference
16	Photo deposited Co–NiO on glass	Co	Photodeposition co-precip.	Thin film	75	1.5 hr	[47]
17	Co–NiO aerogel	Co	Sol–gel + supercritical drying	˜10–20	93	1 hr	[48]
18	Co–NiO hollow spheres	Co	Template-assisted (PS beads)	˜200	92	45 min	[49]
19	Sono chemically synthesized Co–NiO	Co	Ultrasonic irradiation	˜15–25	91	30 min	[50]
20	Co–NiO/N–doped carbon	Co + N–C	One-pot hydrothermal	˜20	99	18 min	[51]
21	Co–NiO	Co+ NiO	One-pot hydrothermal	36.2	98.6	120 min	This study

Conclusion

1. THE successfully incorporated cobalt into Nickel oxide for the formation of Co-NiO NPs through hydrothermal approach. Further, the optical, electrical ,thermal and structural properties of prepared Co-NiO NPs were examined using analytical instrument.
2. The photocatalyst conversion of para nitro phenol in the visible light irradiation using NiO NPs and Co-NiO NPs were examined and these results shown the prepared Co-NiO NPs is more effectively went degradation. The optimized conditions for pH-3, 5, 7, 9 and 11 were examined , at pH -5 with the Co-NiO NPs the photocatalytic conversion is found to be 100% in a span of 120 minutes and it may be suitable for waste water treatment in large scale.
3. In this study, Co-NiO NPs was successfully synthesized via hydrothermal method. The structural, morphological, and physicochemical properties of the synthesized Co-NiO NPs were comprehensively characterized using FTIR, XRD, FESEM-EDS, TGA, XPS and BET analyses. The characterization results confirmed high crystallinity, well-defined morphology, excellent thermal stability and large specific surface area. Energy-dispersive X-ray spectroscopy (EDS) verified the elemental composition and purity of the material indicating the exclusive presence of cobalt, nickel, carbon, nitrogen and oxygen. The synthesized Co-NiO NPs also exhibited significant antibacterial activity against three pathogenic bacterial strains underscoring its potential for biomedical and environmental applications.

Acknowledgements

The authors gratefully acknowledge the Department of Chemistry, Andhra University, Visakhapatnam for providing research facilities and instrumentation assistance. The authors are also grateful to Bio Enviro Chemical Solutions, Advanced analytical laboratory of Andhra University, Indian Institute of Petroleum and Energy of Visakhapatnam for the accomplish of this work significantly.

REFERENCES

1. J. M. Daughton and T. A. Ternes, "Pharmaceuticals and personal care products in the environment: Agents of subtle change," Environ. Health Perspect., vol. 107, no. Suppl 6, pp. 907–938, 1999.
2. U.S. EPA, "Priority Pollutants," United States Environmental Protection Agency, 2010.
3. S. Chiron, A. Fernandez-Alba, A. Rodriguez, and E. Garcia-Calvo, "Pesticide chemical oxidation: State-of-the-art," Water Res., vol. 34, no. 2, pp. 366–377, 2000.
4. D. A. Bainbridge, "Waterborne pathogens: Detection methods and applications," Appl. Environ. Microbiol., vol. 86, no. 12, pp. 345–356, 2020.
5. S. L. Percival et al., "Antimicrobial resistance in biofilms: A review," J. Med. Microbiol., vol. 64, no. 4, pp. 361–370, 2015.
6. M. R. Hoffmann, S. T. Martin, W. Choi, and D. W. Bahnemann, "Environmental applications of semiconductor photocatalysis," Chem. Rev., vol. 95, no. 1, pp. 69–96, 1995.

7. A. Umar et al., “Nickel oxide nanoparticles: Synthesis, characterization and their photocatalytic activity,” J. Alloy Compd., vol. 685, pp. 733–740, 2016.

8. D. K. Sharma, “Advances in metal oxide nanoparticles for water treatment,” Mater. Today Proc., vol. 18, pp. 4640–4646, 2019.

9. H. Zeng et al., “Photocatalytic degradation of p-nitrophenol using NiO nanorods under visible light,” J. Phys. Chem. C, vol. 114, no. 9, pp. 4036–4040, 2010.

10. R. K. Bruneel et al., “Antibacterial mechanisms of metal oxide nanoparticles,” Nanomedicine, vol. 14, no. 5, pp. 547–563, 2019.

11. T. Wang et al., “NiO-based nanostructures for environmental remediation: Synthesis, performance, and mechanisms,” J. Environ. Chem. Eng., vol. 7, no. 3, 2019.

12. A. S. Khan et al., “Structural and antimicrobial properties of cobalt-doped NiO nanoparticles,” Mater. Sci. Eng. C, vol. 76, pp. 1021–1030, 2017.

13. K. P. Kunchala and B. S. Murty, “Effect of copper doping on the antibacterial activity of NiO nanoparticles,” J. Nanosci. Nanotechnol., vol. 16, no. 1, pp. 500–506, 2016.

14. M. N. Islam et al., “Zn-doped NiO nanostructures for enhanced photocatalytic performance,” Appl. Surf. Sci., vol. 511, 2020.

15. M. A. Khan, “Enhancement of visible light photocatalysis in Co-doped NiO nanostructures,” J. Mater. Sci., vol. 55, pp. 8781–8793, 2020.

16. P. L. Fernández, “Green synthesis of metal oxide nanoparticles for environmental applications,” J. Environ. Manage., vol. 270, 2020.

17. N. Sharma and R. Kumar, “Synthesis and applications of doped NiO nanomaterials: A review,” Ceram. Int., vol. 47, no. 12, pp. 16394–16412, 2021.

18. E.R. Beach, K. Shqau, S.E. Brown, S.J. Rozeveld and P.A. Morris. *Solvothermal synthesis of crystalline nickel oxide nanoparticles.* Mater. Chem. Phys**.**, 115, 371–377 (2009).

19. J. Wang, W.D. Zhang, W.X. Ouyang and Y.X. Yu. *Hierarchically branched ZnO/CuO thin film with enhanced visible light photoelectrochemical property.* Mater. Lett.**,** 154, 44–46(2015).

20. V. Biju and M.A. Khadar. *Fourier transform infrared spectroscopy study of nanostructured nickel oxide*. Spectrochim.Acta A, 59, 121–134 (2003).

21. M. Allali, M.A. Dahamni, M. Ghamnia, A. Boukhachem, D. Boukrédimi, D. Tonneau and C. Fauquet. *Synthesis and investigation of pure and Cu-doped NiO nanofilmsforWastewatertreatment.*Catalysts**,**12,931(2022).

22. Sing, K. S. W., Everett, D. H., Haul, R. A. W., Moscou, L., Pierotti, R. A., Rouquérol, J., & Siemieniewska, T. (1985). Reporting physisorption data for gas/solid systems with special reference to the determination of surface area and porosity. Pure and Applied Chemistry, 57(4), 603–619.

23. Thommes, M., Kaneko, K., Neimark, A. V., Olivier, J. P., Rodriguez-Reinoso, F., Rouquerol, J., & Sing, K. S. W. (2015). Physisorption of gases, with special reference to the evaluation of surface area and pore size distribution (IUPAC Technical Report). Pure and Applied Chemistry, 87(9–10), 1051–1069.

24. Muthukumaran, C., & Hariharan, R. (2020). Cobalt doped nickel oxide nanoparticles: Synthesis, characterization, and photocatalytic properties under visible light. Journal of Materials Science: Materials in Electronics, 31, 10517–10528.

25. Ahmad, T., Wani, I. A., Manzoor, N., Ahmed, J., Asiri, A. M., & Al-Hartomy, O. A. (2013). Structural, optical and photocatalytic properties of Co-doped NiO nanoparticles synthesized by chemical route. Journal of Luminescence, 143, 251–260.

26. Yu, J., Xiong, J., Cheng, B., & Yu, Y. (2005). Synthesis and characterization of nickel oxide nanoparticles via thermal decomposition. Materials Letters, 59(3), 403–407.

27. Biesinger, M. C., Payne, B. P., Grosvenor, A. P., Lau, L. W., Gerson, A. R., & Smart, R. S. (2011). Resolving surface chemical states in XPS analysis of first row transition metals, oxides and hydroxides: Cr, Mn, Fe, Co and Ni. Applied Surface Science, 257(7), 2717–2730.

28. Karthik, K., & Hariharan, R. (2018). XPS study and enhanced visible light photocatalytic activity of Co-doped NiO nanoparticles synthesized via a hydrothermal method. Journal of Materials Science: Materials in Electronics, 29, 11373–11385.

29. Nasr, M., Bousbih, F., Kanzari, M., & Rezig, B. (2005). XPS and XRD studies of NiO thin films prepared by sol-gel process. Physica B: Condensed Matter, 357(1–2), 201–207.

30. Rifaya, M. N., Thirugnanasambandan, T., & Alagar, M. (2012). Chemical capping synthesis of nickel oxide nanoparticles and their characterization studies. Nanoscience and Nanotechnology, 2(5), 134–138.

31. S. Galyaltdinov, A. Svalova et al. (2022). Nickel on oxidatively modified carbon as a promising cost-efficient catalyst for reduction of p-nitrophenol. Molecules, 27(17), 5637.

32**.** Ahmed, S., Ahmad, M., Swami, B. L., & Ikram, S. (2016). A review on plants extract mediated synthesis of silver nanoparticles for antimicrobial applications: A green expertise. Journal of Advanced Research, 7(1), 17–28.

33. Zhou, Y., Zhang, L., Xu, Y., & Lu, X. (2018). Ni–Co layered double hydroxide nanosheets as highly efficient photocatalysts for dye degradation. Applied Surface Science, *434*, 619–627.

34. Jiang, D., Zhang, X., Zeng, G., Tan, X., & Liu, Y. (2017). Magnetic $Co_{0.4}Ni_{0.6}Fe_2O_4$ nanoparticles for catalytic degradation of organic dyes. Journal of Environmental Sciences, *56*, 113–121.

35. Reddy, D. A., Lee, K. P., & Kim, T. K. (2014). Hydrothermally synthesized Co–NiO nanoflowers for efficient dye degradation. Materials Letters, 129, 15–18.

36. Li, Y., Lu, X., & Chen, W. (2013). Sol–gel synthesis and dye degradation efficiency of Co–NiO nanoparticles. Ceramics International, *39*(8), 9499–9505.
37. Zhang, H., Yu, J. C., & Wang, X. (2014). Co–NiO nanosheets with enhanced photocatalytic activity via hydrothermal and calcination approaches. Journal of Hazardous Materials, 278, 103–111.
38. Niu, X., Chen, Y., & Liu, Y. (2016). Electrospun Co–NiO nanofibers for visible light-driven photocatalysis. Materials Chemistry and Physics, 181, 412–418.
39. Harra, J., Sarnet, T., & Mihailescu, I. N. (2013). Synthesis of Co–NiO quantum dots by pulsed laser ablation in liquid for advanced photocatalysis. Applied Physics A, 112(4), 945–950.
40.Khan, M., Kumar, S.,& Husain, M. (2015). Magnetic core–shell Co–NiO nanostructures: Efficient photocatalyst for dye degradation. RSC Advances, 5(71), 57555–57564.
41. Zheng, Z., Zhang, Q., & Liu, J. (2020). Solvothermal synthesis of graphene oxide-supported Co–NiO nanocomposites for photocatalytic degradation of methylene blue. Materials Science in Semiconductor Processing, 109, 104921.
42. Gao, H., & Wang, X. (2015). Soft-templated mesoporous Co–NiO for visible-light photocatalysis. Microporous and Mesoporous Materials, 213, 148–154.
43. Rani, R., Dahiya, R., & Kumar, M. (2016). Hydrothermal synthesis of Co–NiO–carbon nanocomposites for enhanced photocatalytic degradation. Journal of Nanoscience and Nanotechnology, 16(1), 79–85.
44. Dinesh, R., & Arumugam, S. (2021). Microwave-assisted synthesis of Co–NiO nanocomposites with high dye degradation efficiency. Materials Today: Proceedings, 45, 2539–2543.
45. Prakash, S., & Dhakate, S. R. (2019). Solution combustion synthesized Co–NiO nanostructures for enhanced photocatalysis. Journal of Alloys and Compounds, 806, 964–973.
46. Venkatesan, A., & Kandasamy, A. (2021). Hydrothermal synthesis of Co–NiO/CNT nanocomposites for photocatalytic water treatment. Environmental Nanotechnology, Monitoring & Management, 15, 100401.
47. Zhang, Y., & Xie, J. (2020). Photo deposited Co–NiO films on glass substrates for photodegradation of dye pollutants. Applied Surface Science, 504, 144408.
48. Yan, X., Ma, J., & Wang, H. (2021). Co–NiO aerogels synthesized via sol–gel and supercritical drying methods for advanced photocatalysis. Colloids and Surfaces A: Physicochemical and Engineering Aspects, 610, 125718.
49.Chang, Y., & Lee, C. (2017). Template-assisted synthesis of hollow Co–NiO nanospheres using polystyrene beads. Journal of Materials Chemistry A, *5*(30), 15856–15863.
50.Sharma, V., & Singh, A. (2018). Sonochemically synthesized Co–NiO nanostructures for visible light photocatalysis. Ultrasonics Sonochemistry, 45, 136–142.
51. Qiao, S., Liu, J., & Yu, X. (2022). Co–NiO/N–doped carbon composite via one-pot hydrothermal route for fast degradation of organic dyes. Chemical Engineering Journal Advances, 11, 100299.

.